JACS
JOURNAL OF THE AMERICAN CHEMICAL SOCIETY
pubs.acs.org/JACS
Article

Taming the Dichalcogenides: Isolation, Characterization, and Reactivity of Elusive Perselenide, Persulfide, Thioselenide, and Selenosulfide Anions

Keyan Li, Lev N. Zakharov, and Michael D. Pluth*

Cite This: J. Am. Chem. Soc. 2023, 145, 13435−13443
Read Online

ABSTRACT: Reactive sulfur species (RSS) and reactive selenium species (RSeS) play integral roles in hydrogen sulfide (H_2S) and hydrogen selenide (H_2Se) biological signaling pathways, and dichalcogenide anions are proposed transient intermediates that facilitate a variety of biochemical transformations. Herein we report the selective synthesis, isolation, spectroscopic and structural characterization, and fundamental reactivity of persulfide (RSS^-), perselenide ($RSeSe^-$), thioselenide ($RSSe^-$), and selenosulfide ($RSeS^-$) anions. The isolated chalcogenides do not rely on steric protection for stability and have steric profiles analogous to cysteine (Cys). Simple reduction of S_8 or Se by potassium benzyl thiolate (KSBn) or selenolate (KSeBn) in the presence of 18-crown-6 afforded [K(18-crown-6)][BnSS] (**1**), [K(18-crown-6)][BnSeSe] (**2**), [K(18-crown-6][BnSSe] (**3**), and [K(18-crown-6][BnSeS] (**4**). The chemical structure of each dichalcogenide was confirmed by X-ray crystallography and solution-state ^1H, ^{13}C, and ^{77}Se NMR spectroscopy. To advance our understanding of the reactivity of these species, we demonstrated that reduction of **1**−**4** by PPh_3 readily generates E═PPh_3 (E: S, Se), and reduction of **1**, **3**, and **4** by DTT readily produces HE^-/H_2E. Furthermore, **1**−**4** react with CN^- to produce ECN^-, which is consistent with the detoxifying effects of dichalcogenide intermediates in the Rhodanese enzyme. Taken together, this work provides new insights into the inherent structural and reactivity characteristics of dichalcogenides relevant to biology and advances our understanding of the fundamental properties of these reactive anions.

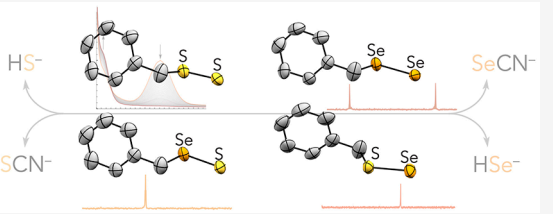

INTRODUCTION

Endogenously produced small gaseous molecules are essential and facilitate a wide array of physiological processes. For example, hydrogen sulfide (H_2S), nitric oxide ($NO^•$), and carbon monoxide (CO) are all established gasotransmitters that play active and expanding roles in complex biological processes such as neural transduction, angiogenesis, and vasodilation.[1,2] More recently, hydrogen selenide (H_2Se) has emerged as a potential new addition to this group due to its integral role in mammalian selenium homeostasis, antioxidant enzyme activity, thyroid functions, and other processes, all of which make selenium an essential inorganic element in the human diet.[3−6] This growing biological significance has catalyzed the recent development of chemical tools for delivery and detection of H_2Se in biology[7−14] and also raised questions about the fundamental reactivity differences of reactive sulfur and selenium species (RSS and RSeS).

The broad utilization of S and Se by Nature is likely due to their versatile redox chemistry with biologically accessible oxidation states spanning from −2 to +6. This redox availability enables the generation of a diverse array of complex and intertwined reactive RSS and RSeS crucial in cellular signaling.[15−17] Established RSS and RSeS typically contain S and Se in the −2 to 0 oxidation states, which provides a duality to these species to act as either pro- or antioxidants. Key RSS examples include H_2S/HS^-, thiols (RSH), persulfides (RSS^-), and organic/inorganic polysulfides ($R_2S_{n>2}$, HSS_n^-), whereas analogous examples of RSeS include H_2Se/HSe^-, selenols (RSeH), thioselenides ($RSSe^-$), and selenotrisulfides (RSSeSR).[15,18] Although S and Se are often considered two of the most similar elements on the periodic table, a number of enzymes rely on Se rather than S for key active site transformations. For example, formate dehydrogenase (FDH), glycine reductase (Grd), and glutathione peroxidase (Gpx) all carry out typically energy intensive transformations and benefit from the enhanced nucleophilicity, better leaving group ability, and lower redox potential of Se over S.[19,20]

Dichalcogenides highlight the intersection of RSS and RSeS with persulfides (RSS^-), thioselenides ($RSSe^-$), and selenosulfides ($RSeS^-$) being proposed intermediates in numerous biochemical processes, whereas perselenides ($RSeSe^-$) have remained primarily a yet-uncharacterized chemical curiosity. RSS^- are the most established dichalcogenides, and

Received: April 11, 2023
Published: June 9, 2023

https://doi.org/10.1021/jacs.3c03766
J. Am. Chem. Soc. 2023, 145, 13435−13443

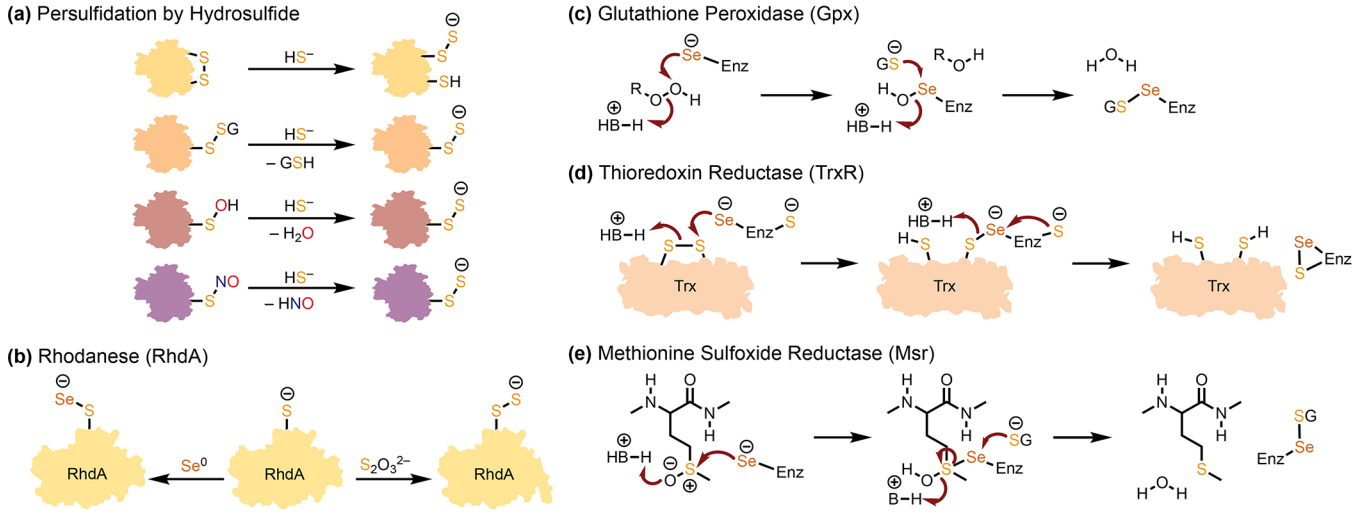

Figure 1. Selected biological pathways for S–S and Se–S bond formation. (a) Persulfidation at oxidized protein thiols, (b) formation of RhdA-bound RSS^- and $RSSe^-$, (c) proposed S–Se bond formation by glutathione peroxidase, (d) thioredoxin reductase, and (e) methionine sulfoxide reductase (Enz-Se^-: enzyme-bound selenocysteine selenolate; GS^-: glutathione thiolate; Trx: thioredoxin; B^+–H: proton source). This figure is based on data, in part, from refs 16 and 17.

glutathione persulfide anion (GSS^-) and cysteine persulfide anion ($CysSS^-$) are both readily generated under physiological conditions.[21,22] Critical biological roles of RSS^- include the construction of iron–sulfur (Fe–S) clusters by the protein scaffold ISCU,[23] detoxification of cyanide (CN^-) by the Rhodanese enzyme (RhdA),[24−26] and mammalian production of H_2S by 3-mercaptopyruvate sulfurtransferase (3-MST).[21,27] As for the more fleeting $RSSe^-$, both glutathione thioselenide ($GSSe^-$) and enzyme-bound thioselenide (Enz-SSe^-) have been postulated as highly reactive intermediates in RhdA prior to reduction to HSe^- or selenophosphate generation.[28] In contrast, the isomeric $RSeS^-$ has been observed crystallographically as a Ni-bound selenocysteine selenosulfide ($SecSeS^-$) in the active site of [NiFeSe] hydrogenase from *Desulfovibrio vulgaris*, which generates hydrosulfide (HS^-) upon reduction.[29] Similarly, a Mo-bound $SecSeS^-$ is a proposed intermediate in the catalytic oxidation of formate by Mo FDH.[30] Finally, $RSeSe^-$ motifs have thus far remained both biologically and chemically elusive, which is likely further confounded by the expected high chemical reactivity of this functional group as well as the trace levels of Se required for biological function. We note that given the rarity and elusiveness of such motifs, the term "perselenide" has been used sporadically in the literature to describe the hetero-dichalcogenide $RSSe^-$ (thioselenide) rather than the more accurate $RSeSe^-$ formulation.

In general, biosynthetic pathways resulting in dichalcogenide formation typically involve the reduction of a partially oxidized S/Se (o.s. ≥ -1) by a fully reduced (o.s. $= -2$) S/Se. For RSS^- generation (persulfidation), the reduction of an oxidized protein thiol (e.g., cysteine disulfide, glutathiolated cysteine, cysteine sulfenic acid, or *S*-nitroso cysteine) by HS^- generates a persulfide, which predominantly exists as RSS^- at physiological pH due to the increased persulfide acidity ($pK_a \approx 6.2$) (Figure 1a).[17,22] Alternatively, protein-bound $CysS^-$ in RhdA can reduce the S^0 of thiosulfate ($S_2O_3^{2-}$) to form $CysSS^-$.[24,25] Persulfidation-like pathways have also been proposed for $RSSe^-$ generation, in which HSe^- reduces oxidized protein thiols to generate $RSSe^-$.[9] Alternatively, glutathione thiolates (GS^-) can reduce oxidized Se to form $GSSe^-$ in RhdA (Figure 1b).[28] Similar reduction of oxidized Se by GS^- has also been proposed in both glutathione peroxidase (Gpx) and methionine sulfoxide reductase (Msr), where enzyme-bound GS-Se-Enz intermediates are likely generated (Figure 1c). Although prior pathways detailing $RSeS^-$ formation are limited, the reduced selenide (Enz-Sec-Se^-) in thioredoxin reductase (TrxR) can reduce the disulfide bridge of thioredoxin to form enzyme-bound Enz-Sec-Se-S intermediates, suggesting that highly nucleophilic selenolate selenocysteine (Sec^-) can reduce sulfane sulfur (S^0) to produce $SecSeS^-$ (Figure 1d,e).[16]

Despite the recognized importance and potential biological roles of these anionic dichalcogenides, the fundamental chemistry of such anions remains essentially unexplored. Our group previously reported the isolation and characterization of the sterically encumbered trityl hydropersulfide (TrtSSH, Trt = Ph_3C), but our prior attempt to access $TrtSS^-$ through deprotonation led to immediate disproportionation to form TrtSH and S_8.[31] Similarly, Nakayama and co-workers have attempted deprotonation of a triptycene-substituted hydroselenosulfide (TrpSeSH), resulting in only the formation of undesirable decomposition products rather than $TrpSeS^-$.[32] Although a Zn-bound $TrtSS^-$ was reported by Artaud and co-workers,[33] the only structurally characterized noncovalently bound RSS^- examples were reported by groups of Rauchfuss and Chen, where reduction of S_8 by PhS^- or $tBuS^-$ provided $PhSS^-$ and $tBuSS^-$, respectively.[34,35] Despite the resonance stabilization from the adjacent Ph substituent in $PhSS^-$ and steric bulk in $tBuSS^-$, the S–S bonds in both species are highly labile in solution and form higher order polysulfides RSS_n^- or the highly colored radical anion $S_3^{\bullet-}$ even at low temperatures. Such complex solution equilibria present further complications in elucidating the reactivities of RSS^-. In the above cases, the need for steric protection of the persulfide motif was heavily emphasized, and attempts to use less sterically bulky analogues with methylene groups adjacent to the dichalcogenide, such as in $CysS^-$, have proven unsuccessful. Highlighting this heightened reactivity, structural characterization of a free $RSSe^-$ species was only reported recently by Chen and co-workers, in which a reaction between NaSPh and Se in the

https://doi.org/10.1021/jacs.3c03766
J. Am. Chem. Soc. 2023, 145, 13435−13443

presence of $[PPh_4][Cl]$ furnished a mixture of $[PPh_4][PhSSe]$ and trace amounts of the accompanying polyselenide $[PPh_4]_2[Se_5]$.[36] Similar to $PhSS^-$, $PhSSe^-$ also exhibits complex in-solution equilibria even at low temperatures, as evidenced by NMR spectroscopy. Further reactivity of this motif was not investigated. To the best of our knowledge, $RSeS^-$ and $RSeSe^-$ motifs have not yet been structurally characterized, although the related perselenanyl radical ($RSeSe^•$) was recently reported by Stalke and co-workers by photolysis of Bn_2Se_2 in the solid state.[37]

Given the biological relevance of these understudied dichalcogenide motifs, we viewed that the direct characterization of $RSSe^-$, $RSeS^-$, RSS^-, and $RSeSe^-$ compounds would provide a useful platform for not only structural characterization but also for probing initial reactivity. Moreover, understanding the chemical reactivity of these compounds could also provide new synthetic strategies to access established H_2S releasing scaffolds such as functionalized selenylsulfides ($RSSeR'$), thioselenic acids ($RSeSH$), and hydropersulfides ($RSSH$).[38] Although prior strategies to stabilize highly reactive S and Se species have often relied on sterically protected substituents,[31,32,39,40] our approach here uses contact ion pairing interactions with complexed alkali metal cations, such as $[K(18\text{-crown-}6)]^+$ and $[Na(15\text{-crown-}5)]^+$, which has previously enabled the isolation of various reactive anions.[41−43] Using this approach, we herein report the syntheses, isolation, characterization, and comparative reactivities of structurally simple RSS^-, $RSeSe^-$, $RSSe^-$, and $RSeS^-$ dichalcogenides.

RESULTS AND DISCUSSION

Synthesis and Characterization. Building from the hypothesis that contact ion pairing could help stabilize anionic dichalcogenides, we treated THF solutions of $[K(18\text{-crown-}6)][BnS]$ or $[K(18\text{-crown-}6)][BnSe]$ generated *in situ* with $^1/_8$ equiv of S_8 or 1 equiv of solid gray Se powder (Scheme 1).

Scheme 1. Synthesis of Dichalcogenides 1−4 (E = S, Se)

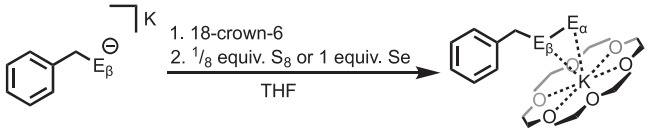

1: E_β = S, E_α = S
2: E_β = Se, E_α = Se
3: E_β = S, E_α = Se
4: E_β = Se, E_α = S

These reaction conditions provided the dichalcogenides $[K(18\text{-crown-}6)][BnSS]$ (**1**), $[K(18\text{-crown-}6)][BnSeSe]$ (**2**), $[K(18\text{-crown-}6][BnSSe]$ (**3**), and $[K(18\text{-crown-}6][BnSeS]$ (**4**), which were characterized by NMR spectroscopy, UV−vis spectroscopy, and X-ray crystallography. The ^1H NMR spectra of **1**−**4** in CD_3CN were well-resolved at room temperature, and no fast exchange or paramagnetic broadening was observed. This stability is contrary to the observation by Chen and co-workers on the solution dynamics of $[PPh_4]$-$[PhSSe]$, which further supports that the typically labile dichalcogenide bonds in **1**−**4** remain intact in solution despite the absence of steric or resonance stabilization. In general, **1**−**4** are stable in the solid state when stored under an inert atmosphere. Multiple attempts to obtain mass spectrometric characterization for **1**, **2**, and **4** proved unsuccessful, indicating their instability upon ionization, particularly in the gas phase. In solution, the terminal Se-containing **2** and **3** exhibit remarkable stability in MeCN, whereas the terminal S-containing **1** and **4** undergo gradual decomposition in solution to form polysulfides and various other decomposition products over the course of a few days.

The ^1H NMR spectra of **1**−**4** display high sensitivity of the benzyl methylene protons to the nearby electronic environments of the dichalcogenide motif. As anticipated, the benzyl proton resonances are shifted more upfield for the S-alkylated anions **1** (3.49 ppm) and **3** (3.57 ppm) than for the Se-alkylated anions **2** (3.66 ppm) and **4** (3.61 ppm). We also used ^{77}Se NMR spectroscopy to further probe the Se electronic environment in **2**−**4**. For perselenide **2**, the ^{77}Se NMR spectrum revealed two resonances at 170.9 and 225.6 ppm corresponding to the terminal (E_α) and internal selenides (E_β) Se atoms, respectively. These peaks are slightly broadened due to unresolved Se−Se and CH_2−Se couplings. For thioselenide **3**, a sharp singlet at 306.2 ppm was observed. This drastic downfield shift when compared to **2** is consistent with our hypothesis that substitution of S for Se at the E_β position should generate a more electron-deficient terminal selenide due to the electronegativity difference between S and Se. Similar differences are observed for the ^{77}Se NMR chemical shifts for E_β positions, in which the ^{77}Se NMR spectrum of **4** shows a sharp triplet at 318.2 ppm that is shifted downfield by nearly 100 ppm when compared to **2** (Figure 2).

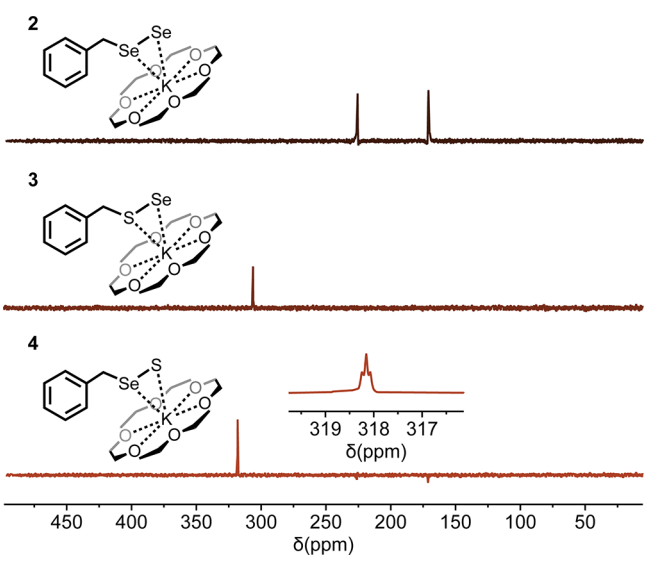

Figure 2. ^{77}Se NMR spectra of **2** (top), **3** (middle), and **4** (bottom) acquired in CD_3CN at 233 K.

The UV−vis spectra of **1**−**4** all show features with moderate bathochromic shifts in the nb → σ^* absorbance with increasing selenium substitution (λ_{max}(**1**): 373 nm, λ_{max}(**2**): 453 nm, λ_{max}(**3**): 418 nm, λ_{max}(**4**): 410 nm). Similar extinction coefficients were observed for compounds **2** and **3** with Se atoms in the E_α position and between compounds **1** and **4** with S atoms in the E_α position (Figure 3a). For selenosulfide **4**, however, the UV−vis spectrum revealed a weak and unexpected absorbance at 610 nm, which we attribute to the radical anion $S_3^{•-}$ formed through equilibrium of **4** with Bn_2Se_2 and inorganic polysulfides. Consistent with this hypothesis, our initial efforts to crystallize **4** led to the

https://doi.org/10.1021/jacs.3c03766
J. Am. Chem. Soc. 2023, 145, 13435−13443

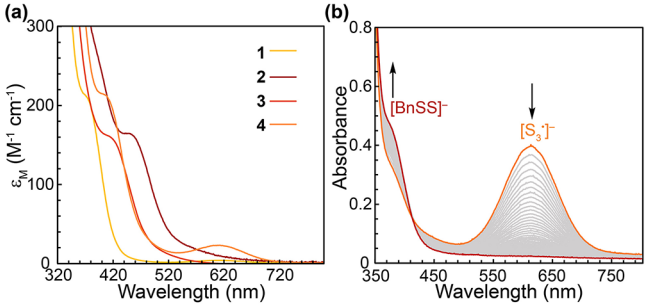

Figure 3. (a) UV−vis spectra of **1**−**4** in MeCN acquired at room temperature. (b) UV−vis trace of the reaction between KSBn and S_8, which shows the diminishing absorbance of $S_3^{\bullet-}$ (λ_{max} = 610 nm) and the emergence of an n.b. to σ^* transition corresponding to **1** (λ_{max} = 373 nm). Spectra were acquired every 2 min.

formation and isolation of the stable polysulfide anion $[K(18\text{-crown-6})]_2[S_4]$, which was isolated and characterized by X-ray crystallography (Figure S40). Further supporting the intermediacy of polysulfide anions in dichalcogenide formation, monitoring the UV−vis spectrum of KSBn treated with S_8 shows a transient absorbance at 610 nm corresponding to $S_3^{\bullet-}$ formation, which bleaches completely upon formation of stable persulfide **1** (Figure 3b).

Structural Analysis. We also characterized dichalcogenides **1**−**4** by X-ray crystallography to confirm our structural assignments and also to better understand structural differences between these reactive anions (Figure 4). Crystals of **1**−

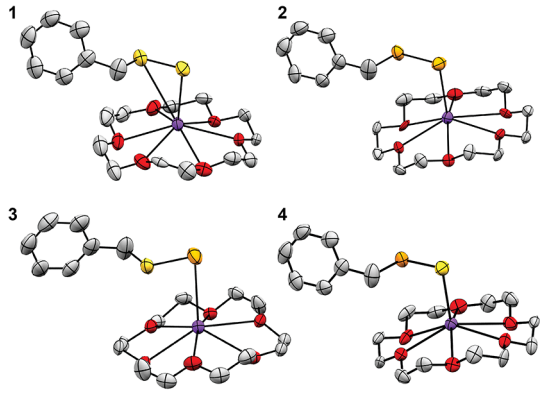

Figure 4. Solid-state structures of **1**−**4**. Purple, red, yellow, orange, and gray ellipsoids represent K, O, S, Se, and C atoms, respectively. Ellipsoids are shown at the 50% probability level. Solvent molecules and H atoms are omitted for clarity.

4 suitable for X-ray diffraction studies were grown by layering of Et_2O onto a saturated solution of **1** in MeCN or by vapor diffusion of Et_2O into a saturated solution of **2**−**4** in MeCN. The S−S distance in **1** is 2.053(2) Å, which is longer than the S−S distances in resonance-stabilized $[PhSS][PPh_4]$ (2.043(11) Å) and shorter than in sterically encumbered $[t\text{BuSS}][PPh_4]$ (2.067(6) Å).[35] The S−S distance in **1** is nearly equivalent to the shortest S−S distance in the dianion $[K(18\text{-crown-6})]_2[S_4]$ (of 2.049(8) Å), which has additional stabilization from two $[K(18\text{-crown-6})]^+$ contact ion pairs.[41] The S−S bond in **1** is longer than neutral S_2-containing species, such as Bn_2S_2 (2.037(5) Å) and TrtSSH (2.039(12) Å).[31,44] This elongated bond distance is consistent with increased electron density in the S−S nonbonding orbital, which promotes destabilizing interactions between the lone pairs. In addition, strong contact-ion pairing interactions are observed between the S−S unit and $[K(18\text{-crown-6})]^+$ as evidenced by the short distances between the terminal (S_α) and internal (S_β) sulfur atoms and the K atom of 3.624(1) and 3.089(2) Å, respectively. The S_β−S_α−K angle of 87.18(6)° also supports that $[K(18\text{-crown-6})]^+$ is interacting with the S_α−S_β unit rather than just the terminal S_α atom.

The Se−Se bond distance of perselenide **2** is 2.322(1) Å, which is significantly longer than the S−S bond in **1** as expected. The Se−Se bond distance in **2** is also longer than that in Bn_2Se_2 (2.315 Å) and $BnSeSe^\bullet$ (2.243 Å),[30] which is consistent with the enhanced lone pair repulsion in anionic **2**. The Se−Se distance of **2**, however, is equivalent to the related dianion $[K(18\text{-crown-6})]_2[Se_4]$ (2.332(1) Å).[42] Much like in the structure of **1**, the terminal (Se_α) and internal (Se_β) selenium atoms both interact with the K atom, with relatively short Se_α−K and Se_β−K distances of 3.215(2) and 3.875(2) Å, respectively. Similar to the structure of **1**, the entire Se_α−Se_β unit appears to interact with the $[K(18\text{-crown-6})]^+$ contact ion, with a Se_β−Se_α−K angle of 87.26(5)°.

Moving to the heterodichalcogenides, thioselenide anion **3** has a S−Se bond distance of 2.214(2) Å, which is longer than the S−Se bond distances in resonance stabilized $[PhSSe][PPh_4]$ of 2.1997(10) Å and for other structurally characterized neutral RSSeR species, which range from 2.125(3) to 2.201(4) Å.[36,45−47] This bond elongation in **3** is consistent with the enhanced destabilizing lone pair repulsion described above. Interactions between the terminal selenium (Se_α) and internal sulfur (S_β) atoms and the K atom are reflected in the short Se_α−K and S_β−K distances of 3.206(1) and 3.798(2) Å, respectively. The Se_α and S_β positions of **3** appear to interact more strongly with $[K(18\text{-crown-6})]^+$ than in **2** but less strongly than in **1**. Similar to the structures of **1** and **2**, the full Se_α−S_β unit interacts with the $[K(18\text{-crown-6})]^+$ contact ion with a S_β−Se_α−K angle of 86.96(4)°.

Lastly, selenosulfide anion **4** has a Se−S bond distance of 2.188(2) Å, which is longer than the Se−S bond in TrpSeSH (2.1796(9) Å) and also the neutral RSSeR species described earlier.[26] Similar interactions between the terminal sulfur (S_α) and internal selenium (S_β) atoms and the K atom are reflected in the short S_α−K and Se_β−K distances of 3.115(3) and 3.728(2) Å, respectively. In addition, similar to the structure of **1**, the entire Se_α−S_β unit appears to interact with the $[K(18\text{-crown-6})]^+$ contact ion, as supported by the S_β−Se_α−K angle of 87.52(7)°.

In addition to the stabilizing interactions offered by $[K(18\text{-crown-6})]^+$, the contact ion interactions also allow for further insights into the electronic environments of E_α and E_β positions in each dichalcogenide. Taking the ratio (R^*) of bond distances (d) E_β−K and E_α−K ($R^* = d_{E\beta K}/d_{E\alpha K}$) allows for direct comparison of E_β−K and E_α−K interactions across structures of **1**−**4**. An R^* value of 1 indicates equal E_β−K and E_α−K interactions, and $R^* > 1$ values signify stronger interactions between K^+ and E_α. Tabulation of R^* values, as well as key structural parameters, are included in Table 1. The average R^* across structures **1**−**4** is 1.190, which indicates that the α and β positions interact with K^+ almost equally with slight preference for the α position. When comparing homodichalcogenides **1** and **2**, perselenide **2** shows a greater R^* value (1.205) than **1** (1.173). The R^* values of **1** and **2** are larger when compared to the related dianions $[K(18\text{-crown-6})]_2[S_4]$ (R^*_{avg} = 0.966, $d_{E\beta K(avg)}$ = 3.275 Å, $d_{E\alpha K(avg)}$ = 3.391 Å,

https://doi.org/10.1021/jacs.3c03766
J. Am. Chem. Soc. 2023, 145, 13435−13443

Table 1. Selected Structural Parameters for 1−4 (E = S, Se)

	$BnSS^-$ (1)	$BnSeSe^-$ (2)	$BnSSe^-$ (3)	$BnSeS^-$ (4)
E_α−E_β (Å)	2.053(2)	2.322(1)	2.214(2)	2.188(2)
C1−E_β (Å)	1.836(6)	1.990(1)	1.846(8)	1.983(8)
E_α−K (Å)	3.089(2)	3.215(2)	3.206(1)	3.115(3)
E_β−K (Å)	3.624(1)	3.875(2)	3.798(2)	3.728(2)
C1−C2(Å)	1.503(9)	1.490(2)	1.497(1)	1.491(1)
$\angle E_\beta E_\alpha K$ (deg)	87.18(6)	87.26(5)	86.96(4)	87.52(7)
R^* ($E_\beta K/E_\alpha K$)	1.173	1.205	1.185	1.197

$\angle E_\beta E_\alpha K_{(avg)}$ = 69.03°, measured using closest K−$S_\alpha S_\beta$ ion pairs) and $[K(18\text{-crown-6})]_2[Se_4]$ (R^*_{avg}= 1.087, $d_{E\beta K(avg)}$ = 3.486 Å, $d_{E\alpha K(avg)}$ = 3.208 Å, $\angle E_\beta E_\alpha K_{(avg)}$ = 76.17°), indicating that the α atoms of dichalcogenides bear significantly more charge than in polychalcogenides. For heterodichalcogenides **3** and **4**, selenosulfide **4** has a larger R^* value (1.197) than **3** (1.185).

Dichalcogenide Reactivity. Having structurally characterized dichalcogenides **1**−**4**, we next aimed to investigate the basic reactivity of these compounds toward simple reductants and electrophiles. Based on the role of RSS^- and $RSSe^-$ as potential biological storage units for fully reduced S^{2-} and Se^{2-} motifs, we first treated **1**−**4** with PPh_3 as a 2e$^-$ reducing agent to determine whether fully reduced S/Se can be liberated. Furthermore, reduction with PPh_3 also allows for direct trapping of the fully reduced chalcogenide in the form of E═PPh_3 (E = S/Se), which can be readily observed by ^{1}H and ^{31}P NMR spectroscopy. Reactions of **1** and **4** with PPh_3 led to the immediate reduction to KSBn and KSeBn, respectively, with generation of S═PPh_3 ($\delta(^{31}P)$ = 42 ppm). Similarly, reduction of **2** and **3** showed analogous formation of the parent chalcogenates and Se═PPh_3 ($\delta(^{31}P)$ = 35 ppm, $^1J_{P-Se}$ = 736 Hz) (Figure 5). Despite the simplicity of this reaction pathway,

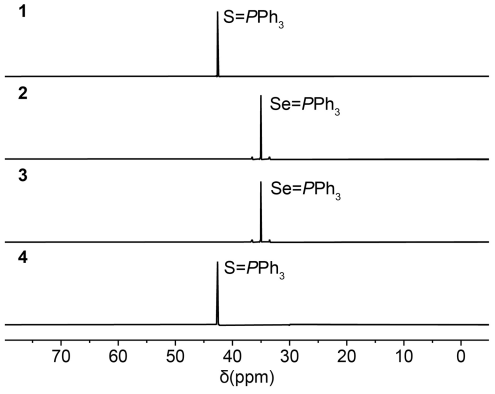

Figure 5. ^{31}P NMR spectra of reactions between **1**−**4** and PPh_3 to produce S═PPh_3 and Se═PPh_3.

prior investigations with the neutral analogue of **1** (BnSSH) toward PPh_3 produced the organic polysulfide BnSSSBn and H_2S rather than the anticipated BnSH and S═PPh_3.[48] This reactivity difference between RSS^- and RSSH highlights the importance of protonation state in moderating persulfide reduction chemistry.

The reduction of RSS^- and $RSSe^-$ to form HS^- and HSe^- has been proposed in the biosyntheses of H_2S and H_2Se by 3-MST and RhdA, respectively. As proxies to this reactivity, we treated **1**−**4** first with dithiothreitol (DTT), which readily converted **1** to form thermodynamically favored cyclic disulfide (DTT_{ox}) and HS^-. Since HS^- formation is not directly observable by ^{1}H NMR due to fast exchange with thiols, addition of BnBr effectively trapped free HS^- as Bn_2S, and the absence of Bn_2S_2 further indicates full consumption of **1** (Figure S14). Similarly, terminal sulfide-containing **4** is also rapidly reduced to form H_2S and BnSeK. Further treatment with PPh_3 failed to generate S═PPh_3, which confirmed the complete reduction of **1** and **4** by DTT. Similar reduction of thioselenide **3** with DTT forms HSe^-, as evidenced by a new peak in the ^{77}Se NMR spectrum at −426.5 ppm (Figure S18). We did not observe a direct reaction of perselenide **2** with DTT even in the presence of excess diisopropylamine. This observation suggests that generation of HSe^- from **2** is not limited to its decreased basicity with increasing Se substitution. The reverse reaction, however, in which highly nucleophilic HSe^- and $BnSe^-$ cooperatively reduce the cyclic disulfide, is likely favored in this scenario. Interestingly, the release of HS^- and HSe^- from **1**−**4** upon treatment with a reducing thiol differs from prior work with isolated neutral RSSH (R: Bn, Ad, Trt) in aprotic solvents, which do not react directly with thiols. This difference in reactivity between isolated RSSH and RSS^- further highlights the important role of protonation states in mediating H_2S release and RSS reactivity.

Dichalcogenides are also hypothesized to play protective roles in RhdA-mediated detoxification of CN^-, and we investigated this reactivity directly by treating $[NBu_4][CN]$ with **1**−**4** in CD_3CN. Addition of $[NBu_4][CN]$ to persulfide **1** or selenosulfide **4** in CD_3CN did not result in an immediate reaction, but allowing the reaction mixture to stir overnight resulted in complete reduction of **1** and **4** to BnSK and BnSeK, respectively. IR spectra of the reaction products showed a strong stretch at 2054 cm^{-1} corresponding to thiocyanate (SCN^-) formation (Figures S32, S35). This reactivity is consistent with the reported biological conversion of CN^- to less toxic SCN^- in RhdA. Performing the analogous reactions with perselenide **2** and thioselenide **3** resulted in immediate conversion to the parent chalcogenates and $SeCN^-$, as evidenced by a new peak in the ^{77}Se NMR spectrum at −307.0 ppm and a new IR stretch at 2062 cm^{-1}, both of which correspond to $SeCN^-$ formation (Figures S33, S34). The enhanced reactivity of terminal selenides **2** and **3** toward CN^- when compared to terminal sulfides **1** and **4** is consistent with the lower reduction potential of Se than S, and this may offer further explanation to the biological utility of $RSSe^-$ in Se-substituted RhdA *in vitro* where detoxification of CN^- by $RSSe^-$ is more facile than RSS^- in S-substituted RhdA.

To investigate whether **1**−**4** could be trapped with suitable electrophiles, we also treated **1**−**4** with BnBr and monitored the reactions by ^{1}H NMR spectroscopy. Addition of 1 equiv of homodichalcogenide **1** or **2** with BnBr in CD_3CN at −35 °C led to the immediate and quantitative conversion to form Bn_2S_2 and Bn_2Se_2, respectively (Figures S22, S24, S25). When performing this reaction with heterodichalcogenides **3** and **4** under similar conditions, we observed formation of expected BnSSeBn but also Bn_2S_2 and Bn_2Se_2 resulting from chalcogen exchange (Figures S28−S31). Similar exchange reactions have been reported previously for RSSeR in the presence of nucleophiles.[49,50] Overall, the direct electrophilic trapping of **1**−**4** further confirms that such species behave as discrete dichalcogenides rather than higher order polychalcogenides in solution. Despite the simplicity of such trapping reactions in isolated system, earlier efforts from our group to trap RSS^- generated *in situ* from RSSH led to capture of higher-order

https://doi.org/10.1021/jacs.3c03766
J. Am. Chem. Soc. 2023, 145, 13435−13443

organic polysulfides, and recent work by Tsui and co-workers to alkylate a related Zn-bound aryltetrasulfanide only yielded thioethers.[51] In addition to clarifying the stability and reactivity of **1**−**4** as discrete dichalcogenides in solution (Figure 6), these data also suggest that such species may function as useful synthons to access other dichalcogenide-containing small molecules.

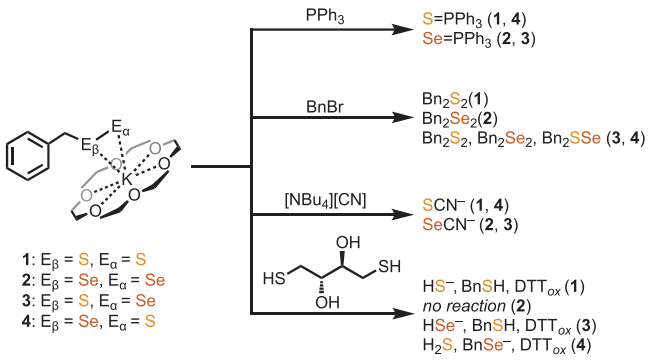

Figure 6. Summary of reactivity of dichalcogenides **1**−**4** toward simple reductants and electrophiles (DTT_{ox}: *trans*-4,5-dihydroxy-1,2-dithiane).

CONCLUSIONS

We demonstrated that the simple incorporation of contact-ion pairing with $[K(18\text{-crown-6})]^+$ provided a facile route to isolate traditionally elusive dichalcogenide anions and enabled the simple synthesis, characterization, and reactivity of a series of biologically relevant dichalcogenides. Our approach also allowed for the first structural characterization of $RSeS^-$ and $RSeSe^-$ species. In particular, the initial isolation of the highly reactive $RSeSe^-$ perselenide hints that reactions between $SecSe^-$ and cellular Se may generate similar reactive intermediates, which could play yet uninvestigated roles in biological Se chemistry, participate in new post-translational modifications, or contribute to bioselenium signaling pathways. Furthermore, we demonstrated that the isolated dichalcogenides react with reductants like PPh_3 and DTT to release reduced chalcogenates and also with $[NBu_4][CN]$ to generate SCN^- and $SeCN^-$, which aligns with the proposed reactivity of these motifs in biology. More broadly, in addition to advancing our understanding of these highly reactive dichalcogenide motifs, we anticipate that access to these simple synthons may enable further bio(in)organic investigations into related RSS and RSeS and advance the important roles of S and Se in biology.

EXPERIMENTAL SECTION

Materials and Methods. All manipulations were carried out in an Inert Atmospheres nitrogen-filled glovebox unless otherwise noted. Chemicals were purchased from TCI, Sigma-Aldrich, VWR International, Acros, Alpha Aesar, or Cambridge Isotopes. Molecular sieves (4 Å) and Celite were activated by heating to 300 °C under vacuum and were stored under N_2. Bulk solvents were deoxygenated and dried by sparging with argon gas followed by passage through an activated alumina column in a Pure Process Technologies solvent system. Solvents are stored over 4 Å sieves under a nitrogen atmosphere. CD_3CN was distilled over K_2CO_3 under N_2 and stored over activated 4 Å sieves prior to use. BnSK was prepared through deprotonation of BnSH with KH in THF. BnSeK was prepared through reduction of Bn_2Se_2 by KBH_4 in CH_2Cl_2/CH_3OH (1:1). UV/vis spectra were acquired on an Agilent Cary 60 UV−vis spectrophotometer equipped with a Quantum Northwest TC-1 temperature controller. NMR spectra were acquired on a Bruker Avance-III-HD 600 spectrometer (^1H: 600 MHz, ^{13}C: 151 MHz, ^{31}P: 242 MHz, ^{77}Se: 115 MHz). Chemical shifts are reported in parts per million (δ) and referenced to residual protic solvent resonances. Mass spectrometry was performed by the Microanalytical Facility at University of Illinois Urbana−Champaign. IR spectra were acquired on a Nicolet 6700 IR spectrometer as KBr pellet samples.

X-ray Crystallography. Diffraction intensities for **1**, **2**, **3**, and **4** were collected at 173 K on a Bruker Apex2 CCD diffractometer using an Incoatec Cu IμS source, Cu Kα radiation, 1.54178 Å. Space groups were determined based on systematic absences. Absorption corrections were applied by SADABS.[52] Structures were solved by direct methods and Fourier techniques and refined on F^2 using full matrix least-squares procedures. All non-H atoms were refined with anisotropic thermal parameters. H atoms in all structures were refined in calculated positions in a rigid group model. All structures are formed in the same non-centrosymmetrical space group $P2_12_12_1$. The Flack parameters are 0.035(9) (**1**), 0.043(14) (**2**), 0.048(9) (**3**), and 0.062(19) (**4**). The $C_{12}H_{24}O_6$ ligand in all structures is disordered over two positions. In **1** and **2** it was refined with restrictions on its geometry: the standard O−C and C−C bond distances were used in the refinement as the targets for corresponding bond lengths. Refinements of occupation factor showed that the ratio between two possible orientations of the ligand is 0.39821/0.60179 (**1**), 0.50642/0.49358 (**3**), and 0.66921/0.33079 (**4**). The structure of **2** was refined with occupation factors for both orientations of the ligand equal to 0.5. In addition to the main molecule with the S−Se−C fragment in **4**, there is also a small amount of molecules with the Se−S−C fragment. The occupation factors of these two species are 0.90557/0.09443, respectively. All calculations were performed by the Bruker SHELXL-2014/7 package.[53]

Syntheses. *[K(18-crown-6)][BnSS] (**1**).* A solution of S_8 (37.3 mg, 0.0146 mmol) in tetrahydrofuran (THF) (2 mL) was added dropwise to another solution containing BnSK (201 mg, 0.123 mmol) and 18-crown-6 (486 mg, 0.184 mmol) in THF (5 mL). The initially clear mixture turned to a teal blue color after each addition, which quickly dissipated to form a cloudy yellow solution. The reaction mixture was allowed to stir for 1 h to produce a pale-yellow solution with a pale-yellow precipitate. The reaction mixture was concentrated to a quarter of its original volume under reduced pressure to promote further precipitation and was subsequently filtered through a pad of Celite. The THF filtrate was discarded. The bright yellow precipitate suspended in Celite was washed into MeCN (2 mL) and was collected through filtration. The pale-yellow filtrate was then layered with Et_2O and stored at −35 °C to produce bright yellow crystals (304 mg, 57%). Crystals suitable for X-ray diffraction were obtained as crystalline plates by layering Et_2O on top of a saturated solution of **1** in MeCN and storing at −35 °C. ^1H NMR (600 MHz, CD_3CN) δ: 7.32 (d, J = 7.3 Hz, 2H, *o*-C*H*), 7.22 (t, J = 7.5 Hz, 2H, *m*-C*H*), 7.13 (t, J = 7.3 Hz, 1H, *p*-C*H*), 3.57 (s, 24H, 18-crown-6), 3.49 (s, 2H, Bn-CH_2). ^{13}C NMR (151 MHz, CD_3CN) δ: 142.3, 129.7, 128.5, 126.6, 70.8, 49.1.

*[K(18-crown-6][BnSeSe] (**2**).* Gray Se powder (30.2 mg, 0.383 mmol) was added to a stirring solution of BnSeK (80.2 mg, 0.383 mmol) and 18-crown-6 (182 mg, 0.690 mmol) in THF (2 mL), and the initially clear orange-yellow mixture turned red-orange with the formation of a red-orange precipitate. The reaction mixture was allowed to stir for 2 h and was concentrated to half of its original volume to promote further precipitation. The reaction mixture was filtered through a pad of Celite, and the THF filtrate was discarded. The orange precipitate suspended in Celite was washed into MeCN (3 mL) and was collected through filtration to yield a deep-red filtrate. The filtrate was layered with Et_2O (5 mL) and stored at −35 °C overnight to afford deep-red crystals. The remaining solvent was removed through filtration to yield **2** as a reflective orange-red powder (150 mg, 71%). Deep-red crystalline blocks suitable for X-ray diffraction were obtained through vapor diffusion of Et_2O into a saturated solution of **2** in MeCN at −35 °C. ^1H NMR (600 MHz,

https://doi.org/10.1021/jacs.3c03766
J. Am. Chem. Soc. 2023, 145, 13435−13443

CD_3CN) δ: 7.31 (d, J = 7.2 Hz, 2H, *o*-C*H*), 7.20 (t, J = 7.3 Hz, 2H, *m*-C*H*), 7.12 (t, J = 7.5, 6.8 Hz, 1H, *p*-C*H*), 3.66 (s, 2H, Bn-CH_2), 3.57 (s, 24H, 18-crown-6). ^{13}C NMR (151 MHz, CD_3CN) δ: 142.5, 128.3, 126.0, 70.2, 31.8. ^{77}Se NMR (115 MHz, CD_3CN) δ: 225.6 (br, CH_2−*Se*−Se), 170.9 (br, CH_2−Se−*Se*).

*[K(18-crown-6)][BnSSe] (**3**).* A suspension of gray Se powder (43.2 mg, 0.544 mmol) in THF (1 mL) was added to a solution of BnSK (95.1 mg, 0.517 mmol) and 18-crown-6 (173 mg, 0.653 mmol) in THF (2 mL). The initially cloudy solution immediately turned to red and then orange. The reaction mixture was stirred overnight to produce an orange solution and an orange precipitate. The reaction mixture was then concentrated to half of its original volume to promote further precipitation and filtered through a pad of Celite. The orange precipitate was washed into minimal MeCN (2 mL) and was filtered to remove Celite to yield a red-orange filtrate. The filtrate was then layered with Et_2O and stored at −35 °C for 2 days to afford large orange crystals, which were collected by decanting the remaining solvents. Drying of the orange crystals *in vacuo* afforded a golden powder (187 mg, 74%). Orange-red block crystals suitable for X-ray diffraction were obtained through vapor diffusion of Et_2O into a concentrated solution of **3** in MeCN. ^{1}H NMR (600 MHz, CD_3CN) δ: 7.33 (d, J = 7.2 Hz, 2H, *o*-C*H*), 7.23 (t, J = 7.3 Hz, 2H, *m*-C*H*), 7.15 (t, J = 6.8 Hz, 1H, *p*-C*H*), 3.57 (s, 24H, 18-crown-6), 3.57 (s, 2H, Bn-CH_2). ^{13}C NMR (151 MHz, CD_3CN) δ: 143.2, 129.5, 128.6, 126.7, 70.9, 46.4. ^{77}Se NMR (115 MHz, CD_3CN) δ: 306.2 (s, CH_2−S−*Se*). HRMS (EI): m/z calcd for $[C_{19}H_{30}KO_6SSe]^+$ 505.0565; found 505.0575.

*[K(18-crown-6][BnSeS] (**4**).* BnSeK (345 mg, 1.65 mmol) and 18-crown-6 (522 mg, 1.98 mmol) were combined in THF (10 mL) to form a homogeneous clear orange solution that was cooled to −78 °C in a cold well in the glovebox. A precooled solution of S_8 (46.0 mg, 0.180 mmol) in THF (5 mL) was added dropwise to the stirring solution over the course of 1 h, during which the initially clear orange solution turned to a teal blue color after each addition. The reaction mixture was allowed to stir for an additional 1 h to produce an orange solution and a yellow precipitate and was warmed to room temperature. The reaction mixture was concentrated to half of its original volume to promote further precipitation and was filtered through a pad of Celite. The THF filtrate was discarded, and the precipitate was suspended in Celite, extracted into cold MeCN (2 mL), and filtered to remove any remaining Celite to afford a greenish-brown filtrate. Layering the filtrate with cold Et_2O (10 mL) and storing at −35 °C resulted in deposition of orange-yellow crystals. The crystals were recrystallized from cold MeCN and Et_2O an additional three times to remove byproducts **2** and **3**. The remaining solvents were removed through filtration to give **4** as a golden powder (128 mg, 15%) Orange-yellow crystals suitable for X-ray diffraction were obtained through vapor diffusion of Et_2O into a concentrated solution of **4** in MeCN at −35 °C for 4 days. ^{1}H NMR (600 MHz, CD_3CN) δ: 7.28 (d, J = 7.5 Hz, 2H, *o*-C*H*), 7.18 (t, J = 7.6 Hz, 2H, *m*-C*H*), 7.08 (t, J = 8.3 Hz, 1H, *p*-C*H*), 3.61 (s, 2H, Bn-CH_2), 3.57 (s, 24H, 18-crown-6). ^{13}C NMR (151 MHz, CD_3CN, 233.2K) δ: 142.0, 128.6, 128.2, 125.9, 70.2, 35.0. ^{77}Se NMR (115 MHz, CD_3CN, 233.2 K) δ: 318.2 (t, J = 9.7 Hz, CH_2−*Se*−S).

*Reduction of **1**−**4** by PPh_3.* PPh_3 (1.1 equiv) in CD_3CN was added to NMR samples of **1**−**4** (1 equiv) in CD_3CN. The NMR samples were shaken after the addition, which resulted in conversion of the initially colored solutions to clear solutions. The NMR tube reactions were subsequently analyzed by ^{1}H and ^{31}P NMR spectroscopy (Figures S12 and S13).

*Reactions of **1**−**4** with DTT.* DTT (1.1 equiv) in CD_3CN was added to NMR samples of **1**−**4** (1 equiv) in CD_3CN. The samples were immediately analyzed by NMR spectroscopy. ^{1}H NMR spectra of DTT-treated **1**, **3**, and **4** all showed the formation of oxidized DTT. The ^{77}Se NMR spectrum of DTT-treated **3** showed the formation of HSe^-. In addition to the direct observation of oxidized DTT in samples containing **1** and **4**, the reaction mixtures were subsequently treated with BnBr to trap liberated HS^- from **1** as Bn_2S, and liberated $BnSe^-$ from **4** was trapped as Bn_2Se (Figures S14−S20). To further verify complete reduction of **1** and **4** by DTT, the NMR samples were then treated with PPh_3. No S=PPh_3 was formed when analyzed by ^{31}P NMR spectroscopy, which confirmed that complete dichalcogenide consumption had occurred.

*Reactions of **1**−**4** with [NBu_4][CN].* [NBu_4][CN] (1.1 equiv) in CD_3CN was added to NMR samples of **1**−**4** (1 equiv) in CD_3CN. Samples containing terminal Se containing **2** and **3** immediately turned clear upon addition of [NBu_4][CN]. Analysis of ^{1}H and ^{77}Se NMR spectra showed complete reduction of **2** and **3** to their parent chalcogenates and $SeCN^-$ (Figures S33 and S34). Samples containing terminal S-containing **1** and **4** did not show immediate conversion to the products, but allowing both samples to stand overnight led to complete conversion of **1** and **4** to their parent chalcogenates and SCN^- (Figures S32−S35).

*Reactions of **1**−**4** with BnBr.* Separate solutions containing **1**−**4** (1 equiv) in CD_3CN were cooled to −25 °C were added dropwise to NMR tubes containing BnBr (1.1 equiv) in cold CD_3CN. The NMR tubes were shaken, during which the initially colored solutions became clear. The final reaction mixtures were subsequently analyzed by NMR spectroscopy (Figures S22, S24, S25, and S28−S31) and were compared with NMR spectra of authentic samples of Bn_2S_2 and Bn_2Se_2 (Figures S23, S26, and S27). Bn_2SSe formation was further verified by HRMS of reaction mixtures. HRMS (EI): m/z calcd for $[C_{14}H_{14}SSe]^+$ 293.9981; found 293.9984.

■ ASSOCIATED CONTENT

Supporting Information

The Supporting Information is available free of charge at https://pubs.acs.org/doi/10.1021/jacs.3c03766.

NMR spectra, IR spectra, crystallographic data (PDF)

Accession Codes

CCDC 2255199−2255202 contain the supplementary crystallographic data for this paper. These data can be obtained free of charge via www.ccdc.cam.ac.uk/data_request/cif, or by emailing data_request@ccdc.cam.ac.uk, or by contacting The Cambridge Crystallographic Data Centre, 12 Union Road, Cambridge CB2 1EZ, UK; fax: +44 1223 336033.

■ AUTHOR INFORMATION

Corresponding Author

Michael D. Pluth − *Department of Chemistry and Biochemistry, Materials Science Institute, Knight Campus for Accelerating Scientific Impact, and Institute of Molecular Biology, University of Oregon, Eugene, Oregon 97403-1253, United States*; orcid.org/0000-0003-3604-653X; Email: pluth@uoregon.edu

Authors

Keyan Li − *Department of Chemistry and Biochemistry, Materials Science Institute, Knight Campus for Accelerating Scientific Impact, and Institute of Molecular Biology, University of Oregon, Eugene, Oregon 97403-1253, United States*

Lev N. Zakharov − *Department of Chemistry and Biochemistry, Materials Science Institute, Knight Campus for Accelerating Scientific Impact, and Institute of Molecular Biology, University of Oregon, Eugene, Oregon 97403-1253, United States*

Complete contact information is available at: https://pubs.acs.org/10.1021/jacs.3c03766

Notes

The authors declare no competing financial interest.

■ ACKNOWLEDGMENTS

We thank the NSF (CHE-2004150 to M.D.P., DGE-2022168 to K.L.) for support of this research.

■ REFERENCES

(1) Wang, R. Two's company, three's a crowd: can H2S be the third endogenous gaseous transmitter? *FASEB J.* **2002**, *16* (13), 1792−1798.
(2) Coletta, C.; Papapetropoulos, A.; Erdelyi, K.; Olah, G.; Módis, K.; Panopoulos, P.; Asimakopoulou, A.; Gerö, D.; Sharina, I.; Martin, E.; Szabo, C. Hydrogen sulfide and nitric oxide are mutually dependent in the regulation of angiogenesis and endothelium-dependent vasorelaxation. *Proc. Natl. Acad. Sci. U.S.A.* **2012**, *109* (23), 9161−9166.
(3) Cupp-Sutton, K. A.; Ashby, M. T. Biological Chemistry of Hydrogen Selenide. *Antioxidants* **2016**, *5* (4), 42.
(4) Mertz, W. The Essential Trace Elements. *Science* **1981**, *213* (4514), 1332−1338.
(5) Kayrouz, C. M.; Huang, J.; Hauser, N.; Seyedsayamdost, M. R. Biosynthesis of selenium-containing small molecules in diverse microorganisms. *Nature* **2022**, *610* (7930), 199−204.
(6) Mueller, E. G. Trafficking in persulfides: delivering sulfur in biosynthetic pathways. *Nat. Chem. Biol.* **2006**, *2* (4), 185−194.
(7) Newton, T. D.; Pluth, M. D. Development of a hydrolysis-based small-molecule hydrogen selenide (H_2Se) donor. *Chem. Sci.* **2019**, *10* (46), 10723−10727.
(8) Newton, T. D.; Bolton, S. G.; Garcia, A. C.; Chouinard, J. E.; Golledge, S. L.; Zakharov, L. N.; Pluth, M. D. Hydrolysis-Based Small-Molecule Hydrogen Selenide (H_2Se) Donors for Intracellular H_2Se Delivery. *J. Am. Chem. Soc.* **2021**, *143* (46), 19542−19550.
(9) Hankins, R. A.; Carter, M. E.; Zhu, C.; Chen, C.; Lukesh, J. C. Enol-mediated delivery of H_2Se from γ-keto selenides: mechanistic insight and evaluation. *Chem. Sci.* **2022**, *13* (44), 13094−13099.
(10) Kang, X.; Huang, H.; Jiang, C.; Cheng, L.; Sang, Y.; Cai, X.; Dong, Y.; Sun, L.; Wen, X.; Xi, Z.; Yi, L. Cysteine-Activated Small-Molecule H_2Se Donors Inspired by Synthetic H_2S Donors. *J. Am. Chem. Soc.* **2022**, *144* (9), 3957−3967.
(11) Kong, F.; Ge, L.; Pan, X.; Xu, K.; Liu, X.; Tang, B. A highly selective near-infrared fluorescent probe for imaging H_2Se in living cells and in vivo. *Chem. Sci.* **2016**, *7* (2), 1051−1056.
(12) Kong, F.; Zhao, Y.; Liang, Z.; Liu, X.; Pan, X.; Luan, D.; Xu, K.; Tang, B. Highly Selective Fluorescent Probe for Imaging H_2Se in Living Cells and in Vivo Based on the Disulfide Bond. *Anal. Chem.* **2017**, *89* (1), 688−693.
(13) Xin, F.; Tian, Y.; Zhang, X. Ratiometric fluorescent probe for highly selective detection of gaseous H_2Se. *Dyes Pigments* **2020**, *177*, 108274.
(14) Hu, B.; Cheng, R.; Gao, X.; Pan, X.; Kong, F.; Liu, X.; Xu, K.; Tang, B. Targetable Mesoporous Silica Nanoprobes for Mapping the Subcellular Distribution of H_2Se in Cancer Cells. *ACS Appl. Mater. Interfaces* **2018**, *10* (20), 17345−17351.
(15) Lau, N.; Pluth, M. D. Reactive sulfur species (RSS): persulfides, polysulfides, potential, and problems. *Curr. Opin. Chem. Biol.* **2019**, *49*, 1−8.
(16) Reich, H. J.; Hondal, R. J. Why Nature Chose Selenium. *ACS Chem. Biol.* **2016**, *11* (4), 821−841.
(17) Mishanina, T. V.; Libiad, M.; Banerjee, R. Biogenesis of reactive sulfur species for signaling by hydrogen sulfide oxidation pathways. *Nat. Chem. Biol.* **2015**, *11* (7), 457−464.
(18) Weekley, C. M.; Harris, H. H. Which form is that? The importance of selenium speciation and metabolism in the prevention and treatment of disease. *Chem. Soc. Rev.* **2013**, *42* (23), 8870−8894.
(19) Stadtman, T. C. Selenium Biochemistry. *Science* **1974**, *183* (4128), 915−922.
(20) Stadtman, T. C. Selenium-Dependent Enzymes. *Annu. Rev. Biochem.* **1980**, *49* (1), 93−110.
(21) Filipovic, M. R.; Zivanovic, J.; Alvarez, B.; Banerjee, R. Chemical Biology of H_2S Signaling through Persulfidation. *Chem. Rev.* **2018**, *118* (3), 1253−1337.
(22) Everett, S. A.; Folkes, L. K.; Wardman, P.; Asmus, K. D. Free-Radical Repair by a Novel Perthiol: Reversible Hydrogen Transfer and Perthiyl Radical Formation. *Free Radic. Res.* **1994**, *20* (6), 387−400.
(23) Braymer, J. J.; Lill, R. Iron−sulfur cluster biogenesis and trafficking in mitochondria. *J. Biol. Chem.* **2017**, *292* (31), 12754−12763.
(24) Westley, J. Rhodanese. In *Advances in Enzymology and Related Areas of Molecular Biology*; John Wiley & Sons, Ltd, 1973; pp 327−368.
(25) Nandi, D. L.; Horowitz, P. M.; Westley, J. Rhodanese as a thioredoxin oxidase. *Int. J. Biochem. Cell Biol.* **2000**, *32* (4), 465−473.
(26) Ploegman, J. H.; Drent, G.; Kalk, K. H.; Hol, W. G. J.; Heinrikson, R. L.; Keim, P.; Weng, L.; Russell, J. The covalent and tertiary structure of bovine liver rhodanese. *Nature* **1978**, *273* (5658), 124−129.
(27) Kimura, Y.; Koike, S.; Shibuya, N.; Lefer, D.; Ogasawara, Y.; Kimura, H. 3-Mercaptopyruvate sulfurtransferase produces potential redox regulators cysteine- and glutathione-persulfide (Cys-SSH and GSSH) together with signaling molecules H_2S_2, H_2S_3 and H_2S. *Sci. Rep.* **2017**, *7* (1), 10459.
(28) Ogasawara, Y.; Lacourciere, G.; Stadtman, T. C. Formation of a selenium-substituted rhodanese by reaction with selenite and glutathione: Possible role of a protein perselenide in a selenium delivery system. *Proc. Natl. Acad. Sci. U.S.A.* **2001**, *98* (17), 9494−9498.
(29) Marques, M. C.; Coelho, R.; Pereira, I. A. C.; Matias, P. M. Redox state-dependent changes in the crystal structure of [NiFeSe] hydrogenase from Desulfovibrio vulgaris Hildenborough. *Int. J. Hydrogen Energy* **2013**, *38* (21), 8664−8682.
(30) Mota, C. S.; Rivas, M. G.; Brondino, C. D.; Moura, I.; Moura, J. J. G.; González, P. J.; Cerqueira, N. M. F. S. A. The mechanism of formate oxidation by metal-dependent formate dehydrogenases. *J. Biol. Inorg. Chem.* **2011**, *16* (8), 1255−1268.
(31) Bailey, T. S.; Zakharov, L. N.; Pluth, M. D. Understanding Hydrogen Sulfide Storage: Probing Conditions for Sulfide Release from Hydrodisulfides. *J. Am. Chem. Soc.* **2014**, *136* (30), 10573−10576.
(32) Ishii, A.; Takahashi, T.; Tawata, A.; Furukawa, A.; Oshida, H.; Nakayama, J. First synthesis and characterization of isolable thioselenenic acid, triptycene-9-thioselenenic acid. *Chem. Commun.* **2002**, *23*, 2810−2811.
(33) Galardon, E.; Tomas, A.; Selkti, M.; Roussel, P.; Artaud, I. Synthesis, Characterization, and Reactivity of Alkyldisulfanido Zinc Complexes. *Inorg. Chem.* **2009**, *48* (13), 5921−5927.
(34) Krautscheid, U.; Dev, S.; Krautscheid, H.; Paul, P. P.; Wilson, S. R.; Rauchfuss, T. B. N-Methylimidazole Mediated Chemistry of Transition Metal Phenylthiolates. The Isolation of the Perthiolate Salts $[M(N\text{-}MeIm)_6](S_2Ph)_2$. *Z. Naturforsch. B* **1993**, *48* (5), 653−658.
(35) Jungen, S.; Paenurk, E.; Chen, P. Synthesis, Spectroscopic, and Structural Characterization of Organyl Disulfanides and a Tetrasulfanide. *Inorg. Chem.* **2020**, *59* (17), 12322−12336.
(36) Jungen, S.; Chen, P. Synthesis, Isolation, and Characterization of a Phenylsulfane-Selenolate Compound. *Inorg. Chem.* **2020**, *59* (18), 13315−13319.
(37) Schürmann, C. J.; Teuteberg, T. L.; Stückl, A. C.; Ruth, P. N.; Hecker, F.; Herbst-Irmer, R.; Mata, R. A.; Stalke, D. Trapping X-ray Radiation Damage from Homolytic Se−C Bond Cleavage in BnSeSeBn Crystals (Bn = benzyl, $CH_2C_6H_5$). *Angew. Chem., Int. Ed.* **2022**, *61* (26), e202203665.
(38) Hamsath, A.; Xian, M. Chemistry and Chemical Biology of Selenenyl Sulfides and Thioseleninic Acids. *Antioxid. Redox Signal.* **2020**, *33* (16), 1143−1157.
(39) Shimada, K.; Goto, K.; Kawashima, T.; Takagi, N.; Choe, Y.-K.; Nagase, S. Isolation of a Se-Nitrososelenol: A New Class of Reactive

Nitrogen Species Relevant to Protein Se-Nitrosation. *J. Am. Chem. Soc.* **2004**, *126* (41), 13238−13239.
(40) Goto, K.; Sonoda, D.; Shimada, K.; Sase, S.; Kawashima, T. Modeling of the 5′-Deiodination of Thyroxine by Iodothyronine Deiodinase: Chemical Corroboration of a Selenenyl Iodide Intermediate. *Angew. Chem.* **2010**, *122* (3), 555−557.
(41) Smiles, D. E.; Wu, G.; Hayton, T. W. Reversible Chalcogen-Atom Transfer to a Terminal Uranium Sulfide. *Inorg. Chem.* **2014**, *53* (24), 12683−12685.
(42) Smiles, D. E.; Wu, G.; Hayton, T. W. Synthesis of Terminal Monochalcogenide and Dichalcogenide Complexes of Uranium Using Polychalcogenides, $[En]^{2-}$ (E = Te, n = 2; E = Se, n = 4), as Chalcogen Atom Transfer Reagents. *Inorg. Chem.* **2014**, *53* (19), 10240−10247.
(43) Hosseininasab, V.; Bertke, J. A.; Warren, T. H. Thionitrite and Perthionitrite in NO Signaling at Zinc. *Angew. Chem., Int. Ed.* **2021**, *60* (39), 21184−21188.
(44) van Dijk, B.; Visser, G. J. Note on the space group of dibenzyl disulphide. *Acta Cryst. B* **1971**, *27* (4), 846.
(45) Illyés, T.-Z.; Balla, S.; Bényei, A.; Kumar, A. A.; Timári, I.; Kövér, K. E.; Szilágyi, L. Exploring the Syntheses of Novel Glycomimetics. Carbohydrate Derivatives with Se-S- or Se-Se-Glycosidic Linkages. *ChemistrySelect* **2016**, *1* (10), 2383−2388.
(46) du Mont, W.-W.; Mugesh, G.; Wismach, C.; Jones, P. G. Reactions of Organoselenenyl Iodides with Thiouracil Drugs: An Enzyme Mimetic Study on the Inhibition of Iodothyronine Deiodinase. *Angew. Chem., Int. Ed.* **2001**, *40* (13), 2486−2489.
(47) Figliola, C.; Male, L.; Horton, P. N.; Pitak, M. B.; Coles, S. J.; Horswell, S. L.; Grainger, R. S. [FeFe]-Hydrogenase Synthetic Mimics Based on Peri-Substituted Dichalcogenides. *Organometallics* **2014**, *33* (17), 4449−4460.
(48) Bailey, T. S.; Pluth, M. D. Reactions of isolated persulfides provide insights into the interplay between H_2S and persulfide reactivity. *Free Radical Biol. Med.* **2015**, *89*, 662−667.
(49) Canal-Martín, A.; Pérez-Fernández, R. Biomimetic selenocystine based dynamic combinatorial chemistry for thiol-disulfide exchange. *Nat. Commun.* **2021**, *12* (1), 163.
(50) Steinmann, D.; Nauser, T.; Koppenol, W. H. Selenium and Sulfur in Exchange Reactions: A Comparative Study. *J. Org. Chem.* **2010**, *75* (19), 6696−6699.
(51) Seo, W. T. M.; Ballesteros, M.; Tsui, E. Y. Sulfane Decreases the Nucleophilic Reactivity of Zinc Thiolates: Implications for Biological Reactive Sulfur Species. *J. Am. Chem. Soc.* **2022**, *144* (45), 20630−20640.
(52) Sheldrick, G. M. *Bruker/Siemens Area Detector Absorption Correction Program*; Bruker AXS: Madison, WI, 1998.
(53) Sheldrick, G. M. Crystal Structure Refinement with SHELXL. *Acta Crystallogr.* **2015**, *C71*, 3−8.

https://doi.org/10.1021/jacs.3c03766
J. Am. Chem. Soc. 2023, 145, 13435−13443